Acta Crystallographica Section D
Biological Crystallography
ISSN 0907-4449

Crystallization and phasing of alanine dehydrogenase from *Archaeoglobus fulgidus*

Natasha Smith,[a] Martin Mayhew,[b] Howard Robinson,[c] Annie Héroux,[c] David Charlton,[d] Marcia J. Holden[a] and D. T. Gallagher[a]*

[a]Biotechnology Division of the National Institute of Standards and Technology, Gaithersburg, MD 20899-8312, USA, [b]Biocatalytics, Inc., Pasadena, CA 91105, USA, [c]Biology Department, Brookhaven National Laboratory, Upton, NY 11973, USA, and [d]Department of Computer Science, Carnegie-Mellon University, Pittsburgh, PA, USA

Correspondence e-mail: travis.gallagher@nist.gov

Received 27 May 2003
Accepted 29 September 2003

Alanine dehydrogenase (AlaDH) from the hyperthermophilic archaeon *Archaeoglobus fulgidus* is a dimer of 35 kDa chains. The archaeal enzyme appears to represent a new class of AlaDH that is not homologous to bacterial AlaDH enzymes, but has close evolutionary links to the broad ornithine cyclodeaminase/μ-crystallin family, which includes human thyroid hormone binding protein, which has 30% sequence identity to the *A. fulgidus* gene. The enzyme has been cloned, shown to catalyze the NAD-dependent interconversion of alanine and pyruvate and crystallized in several forms. Although the purified protein crystallized readily under many conditions, most of the crystals diffracted weakly or not at all. One polymorph growing in space group $P2_12_12_1$ has non-crystallographic symmetry that becomes crystallographic, changing the space group to $P2_12_12$, upon binding iridium or samarium. Before and after derivatization, these crystals diffracted to 2.5 Å using synchrotron radiation. Multiwavelength diffraction data were collected from the non-isomorphous iridium derivative, enabling structure determination.

1. Introduction

The interconversion of alanine and pyruvate is central to metabolism, serving energy production in the oxidative forward direction and anabolic growth in the reductive direction, yielding alanine. AlaDH enzymes from a variety of bacteria have been characterized (Hutter & Singh, 1999; Galkin *et al.*, 1999). Most are hexameric; tetramers and octamers have also been reported. The crystal structure of the hexameric AlaDH with bound NAD from *Phormidium lapideum* has been reported (Baker *et al.*, 1998; PDB code 1pjc). The sequence of the AlaDH from *Archaeoglobus fulgidus* was reported along with the organism's complete genome (Klenk *et al.*, 1997). The 322-residue sequence has no significant homology with previously reported AlaDHs, although the NAD-binding motif G*x*G*xx*G/A shared by most Rossmann-fold dehydrogenases (Rao & Rossmann, 1973) is present starting at Gly132. The gene (TIGR: AF1665) has been annotated as a putative ornithine cyclodeaminase (OCD) based on its homology to the OCD/μ-crystallin family. Biochemical characterization has shown that the homodimer lacks OCD activity and is in fact an NAD-dependent AlaDH (Schroeder *et al.*, 2003). The *A. fulgidus* enzyme thus appears to represent a new class of AlaDH that is non-homologous to bacterial AlaDH enzymes but instead belongs to the phyletically broad μ-crystallin family. Homologous members of this family include cyclodeaminase enzymes in eubacteria (Khaw *et al.*, 1998), eye-lens proteins in marsupials (Chang & Lee, 1994) and thyroid hormone binding protein in human retina and other tissues (Segovia *et al.*, 1997).

Crystallographic imaging of protein molecules requires that two problems lacking general solutions must be solved for each new protein: crystallization and phasing. The two problems are coupled; the difficulty of the second problem depends on the quality of the solution to the first, *i.e.* the quality of the native crystals. When only mediocre crystals have appeared, the most direct route to interpretable electron density may be by derivatization, data collection and phase calculation using existing crystals; alternatively, the best strategy may be to continue crystal screening, seeking superior crystals *via* improved conditions or new conditions (*i.e.* a new polymorph). This paper reports the crystallization and phase determination of alanine dehydrogenase with bound NAD from the hyperthermophilic archeon *A. fulgidus*. Because in this case the phasing involved analysis of multiple polymorphs, the crystallization and derivatization are reported together. A description of the refined structure will be published separately.

2. Cloning and protein preparation

The gene for alanine dehydrogenase from *A. fulgidus* was cloned by PCR amplification of genomic DNA isolated from *A. fulgidus* cells. Restriction endonuclease sites for *Nde*I (forward) and *Bam*HI (reverse) were added to the 5′ end of the primers. The PCR product was purified, restricted and ligated into the vector pRE1 (Reddy *et al.*, 1989). The sequence was verified to be the same as AF1665 by DNA sequencing using a 373 DNA Sequencer (Applied Biosystems, Foster City, CA, USA) with Dye Terminator Cycle Sequencing chemistry. *Escherichia coli* MZ1 cells were transformed with the vector pMHAF1 (pRE1/AF1665). Cells were cultured at 303 K and expression of the alanine dehydrogenase protein was initiated during log-phase growth by a heat jump to 314 K. Cells were harvested at stationary phase.

Alanine dehydrogenase protein was purified from the bacterial cell lysate, with incubation at 353 K for 1.5 h as the first step. The heat-treated extract was centrifuged to remove the precipitated heat-sensitive *E. coli* proteins and loaded onto a DEAE Sepharose (Amersham Pharmacia Biotech, Piscataway, NJ, USA) ion-exchange column equilibrated with a buffer consisting of 20 m*M* Tris–HCl and 1 m*M* DTT (dithiothreitol) pH 8.2. The column was washed with 2 l of the same buffer and alanine dehydrogenase was eluted with a NaCl gradient (0–1 *M*) in the same buffer. The presence of alanine dehydrogenase in column fractions was determined by enzyme assay and relevant column fractions were pooled based on enzyme assay and polyacrylamide gel electrophoresis. The pooled fractions were concentrated to 5–8 ml and applied to a Sephacryl S-200HR gel-filtration column (Amersham Pharmacia Biotech, Piscataway, NJ, USA). Relevant fractions for the final protein preparation were determined by activity assays and were checked for contaminating proteins by gel electrophoresis. The final product was assayed for activity and the protein concentration was determined using the Bio-Rad Protein Assay (Bio-Rad Laboratories, Hercules, CA, USA) with BSA as a standard. Enzyme activity was assayed by following the oxidation of NADH at 340 nm (ε_{340} = 6.22 mM^{-1} cm^{-1}) on a Beckman DU-650 spectrophotometer (Beckman Coulter, Fullerton, CA, USA). Assays were conducted at 295 K in a reaction mixture (1 ml) consisting of 50 m*M* Tris–HCl, 0.2 *M* $(NH_4)_2SO_4$, 12.5 m*M* pyruvate plus protein at pH 8.2. The reaction was started with the addition of 50 µl of 3 m*M* NADH.

Table 1
Crystal forms of *A. fulgidus* AlaDH.

All buffer concentrations are 100 m*M*. Diffraction resolutions were determined by visual inspection using a rotating-anode diffractometer and MAR image-plate detector, except for those in parentheses, which are synchrotron values. Resolutions were measured for crystals frozen with 20% MPD (methylpentanediol) added, except for conditions that already included MPD. Crystal growth was at 297 K unless otherwise specified.

			Unit-cell parameters					
Crystal form	Shape	Space group	*a* (Å)	*b* (Å)	*c* (Å)	*β* (°)	Growth conditions†	Resolution (Å)
Form 1	Blocks	*I*4	64	64	360		5% PEG 6K, NaCit pH 4.0	4
Form 2	Rhombohedra	—					20% PEG 8K, 300 m*M* $MgAc_2$, NaCac pH 6.0, 277 K	10
Form 3	Long bars	Orthorhombic	55	84	174		25% PEG 4K, NaCit pH 6.0	3.5
Form 4	Rhombic plates	$P2_12_12$	55	132	95		0–20% PEG 4K, Ac or MES pH 4.8	3.2
Form 5	Bars	$P2_12_12_1$	95	110	138		25% MPD, 0.2 *M* NaCl, NaAc pH 4.2, 277 K	3.0 (2.5)
Form 6	Bars	$P2_12_12$	93	137	55		Form 5 + Sm or Ir	3.0 (2.5)
Form 7	Bars	—					10% PEG 8K, Tris pH 8.5	6
Form 8	Irregular	*C*2	109	55	131	111	MPD, see text	2.8 (2.3)

† Abbrevations: Cit, citrate; DTT, dithiothreitol; Cac, cacodylate; Ac, acetate; MES, 2-morpholinoethanesulfonic acid; MPD, 2-methyl 2,4,-pentanediol; PEG, polyethylene glycol.

3. Crystal growth and derivatization

Protein was prepared for crystallization by concentration to 15 mg ml^{-1} (0.2 m*M* dimer) in a buffer comprising 10 m*M* Tris pH 7.5, 100 m*M* NaCl. The redox cofactor NAD was added at 0.6 m*M*. Initial screening was performed with Crystal Screen 1 from Hampton Research at both room temperature (∼297 K) and 277 K, using hanging drops. These screens gave an unusually high yield, with about 20% of the 98 conditions producing crystals of some kind. The two temperatures were equally successful and most of the crystals appeared at both temperatures. It was also observed that including 2 m*M* DTT improved most of the crystals (subsequent analysis has shown that the protein's three cysteines are not exposed, so the mechanism of DTT improvement of crystal growth appears to be independent of cysteine interactions). Despite the abundance of crystals, most of them diffracted inadequately (see Table 1).

Conditions for forms 1–3 (Table 1) were obtained by optimizing crystallogenic conditions from the initial screens. The prevalence of PEG in those conditions led to further screening that revealed the other forms. Form 4 crystals grew from very low PEG concentrations, even including unmixed protein solution (zero PEG), when suspended over slightly hygroscopic low-pH wells. Form 5 was the first polymorph considered worth the investment of deriva-

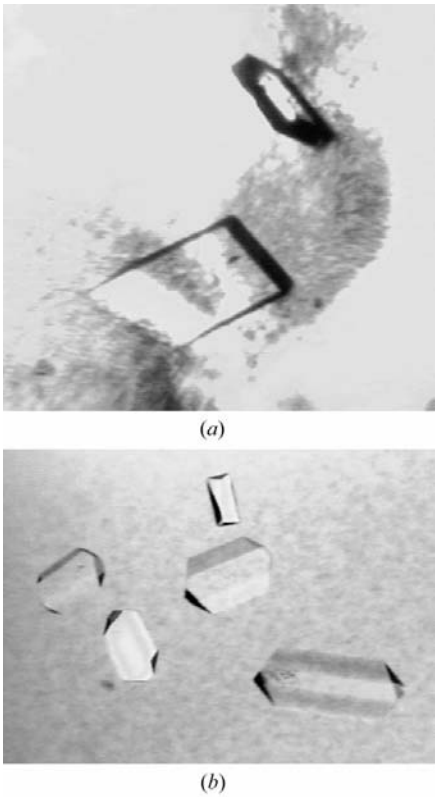

Figure 1
Photographs of the two best diffracting crystal forms. The orthorhombic crystals in (*a*) (form 5) undergo a space-group change (with no change in visual appearance) on derivatization by Ir or Sm (see text). The crystals in (*b*) belong to space group *C*2 (form 8) and are the best diffractors yet found, with diffraction extending to 2.3 Å resolution.

Table 2
Multiwavelength diffraction statistics.

Values in parentheses refer to the outermost resolution shell used (2.94–2.80 Å).

Data set	Peak	Inflection	Remote
Wavelength (Å)	1.1048	1.1051	1.0880
Observations	126513	229070	193711
Unique reflections	17822	17876	17854
Resolution range (Å)	30–2.8	30–2.8	30–2.8
Completeness (%)	99 (99)	99 (99)	99 (99)
Redundancy	7.1 (6.2)	12.8 (11.1)	10.8 (9.7)
$I/\sigma(I)$	18.6 (14.3)	20.1 (14.9)	19.4 (15.1)
$R_{\rm merge}$†	0.06 (0.19)	0.06 (0.18)	0.06 (0.19)

† $R_{\rm merge} = \sum |I - \langle I \rangle| / \sum I$.

tive screening. Although this form has the drawbacks of low pH and two dimers per asymmetric unit, its diffraction was better than previous forms, it freezes well and it has a favorable space group ($P2_12_12_1$). Optimized cultivation involved pipet-based microseeding (using seeds produced by crushing a small crystal using a pipet tip, then diluting 10^4–10^8-fold in pH 5 well solution and delivery in a 0.5 µl volume by pipet) into pH 5.0 drops that were then suspended over pH 4.2 wells. Native

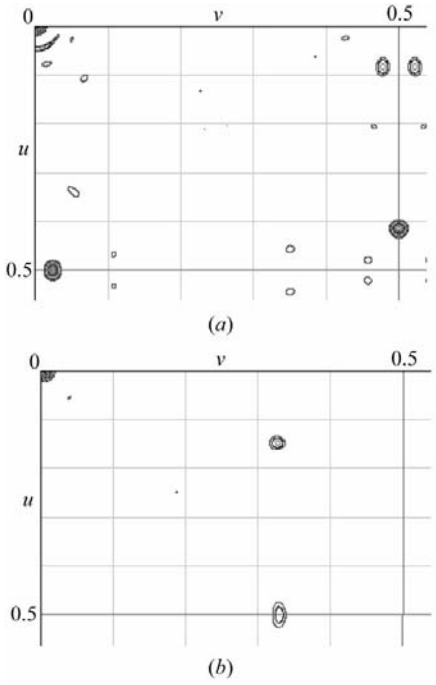

Figure 2
Anomalous difference Patterson maps from the Sm and Ir derivatives. In (*a*), the $w = 0$ Harker section of the Sm-derivative anomalous difference Patterson, calculated in the 30–3 Å resolution range and contoured at intervals of 3σ, shows the *xy* position of the Sm site at (0.04, 0.23, 0.01). In (*b*), the analogous section from the Ir derivative (Ir site at 0.43, 0.16, 0.15). Although the two metals produce the same change in crystal symmetry, they clearly bind at different sites.

Table 3
Anomalous difference correlation for wavelength pairs.

Values given are the standard correlation coefficient between corresponding intensities in two data sets as calculated by *SOLVE*. They serve as a practical approximate indicator of anomalous signal strength.

Resolution shell (Å)	Peak/ inflection	Inflection/ remote	Peak/ remote
30–5.9	0.86	0.83	0.78
5.9–4.1	0.70	0.63	0.56
4.1–3.7	0.54	0.50	0.41
3.7–3.4	0.46	0.38	0.32
3.4–3.1	0.31	0.27	0.21
3.1–2.9	0.23	0.16	0.17
Overall	0.56	0.50	0.42

Patterson maps (Patterson, 1934) contained a strong peak at 0, $\frac{1}{2}$, 0, indicating that the non-crystallographic symmetry includes a dyad along *b* (which, together with the crystallographic screw along *b*, produces the observed peak). Further evidence of this pseudosymmetry was a pattern of alternating strong and weak reflections along *k* for low *h* and *l*. Fig. 1(*a*) is a photograph of form 5 crystals. Extensive screening of these crystals against heavy-metal solutions yielded no suitably diffracting isomorphous derivatives; however, form 5 crystals are converted to form 6 by binding either Sm or Ir ions, although at different locations (see below). The appearance of the crystals was unaffected by the transformation.

4. Diffraction and phasing

Although no isomorphous derivatives were found, overnight soaking with either 5 m*M* $SmCl_3$ or 5 m*M* $IrCl_3$ was found to alter the space group of form 5 crystals by converting the NCS dyad along *b* into a crystallographic dyad. This has the effect of halving the *b* unit-cell parameter, reducing the size of the asymmetric unit to a single dimer, changing the space group to $P2_12_12$ and reordering the axes to follow the convention of unique axis last, to produce form 6 (Table 1). Diffraction data sets were collected for both Sm- and Ir-treated crystals that underwent this space-group change. Although the space-group conversion was the same for the two metals, anomalous difference Patterson maps show that the metals produce the effect by binding at different locations. Fig. 2 shows the $u = 1/2$ sections of the maps for these two data sets. The derivative crystals now have only a dimer in the asymmetric unit. The direction of this remaining NCS axis cannot be inferred from self-rotation function (Rossmann, 1972) analysis, because it coincides closely with the *a* direction. However, it can be seen in the self-Patterson map from these data (Fig. 3).

With the anomalous Patterson map's indication that Ir was bound to AlaDH (Fig. 2*b*), the crystals were utilized for three-wavelength (MAD) phasing (Pahler *et al.*, 1990) at Brookhaven National Laboratory beamline X26c (Table 2). These data, limited to 2.9 Å resolution, were used in the program *SOLVE* (Terwilliger & Berendzen, 1999), which calculated the correlations among the anomalous differences at the three wavelengths given in Table 3. The automatic chain-tracing feature made the local dyad easy to discern. With the NCS included in the automatic chain tracing, *SOLVE* correctly traced 52% of the 644 residues in the asymmetric unit. Subsequent manual model building using the program *Xfit* (McRee, 1999) led to a nearly complete chain trace (96%). Since many of the side chains were still truncated at this point (*e.g.* modeled as Ala when known to be Lys), the atom fraction of 4134 out of 4898 is a better measure of the model's completeness. This model, before any refinement, had an *R* value of 0.45 in the resolution range 10–4 Å.

Meanwhile, continued efforts to produce better crystals had led to a new polymorph, form 8, in space group *C*2 (Fig. 1*b*, Table 1). These crystals were grown by mixing a 2 µl droplet of protein solution with half its

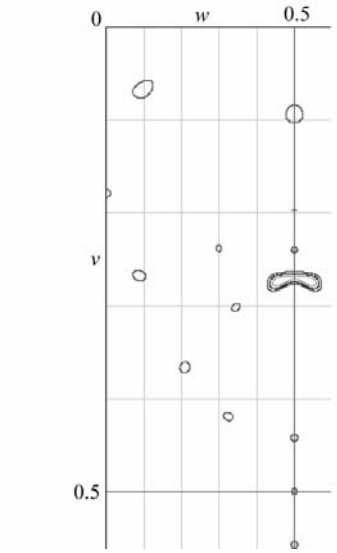

Figure 3
Native Patterson of the Ir-derivative data. The $u = 1/2$ section is calculated at 10–3 Å resolution and contoured at intervals of 3σ. The peak at 0.5, 0.27, 0.46 arises from translation owing to the combination of the crystallographic screw along *a* and the non-crystallographic dimer axis nearly parallel to *a*. The location of the peak gives the approximate *yz* position of the molecular dyad as 0.11, 0.23. The analogous map for the Sm derivative has a peak at the same location.

volume of 20% MPD and suspending over 20% MPD buffered with sodium acetate to pH 4.9. The *C*2 crystals gave significantly higher resolution diffraction than previously characterized forms, *i.e.* to 2.3 Å resolution. They had one dimer per asymmetric unit and a V_M of 2.64 Å^3 Da^{-1}, compared with 2.53 Å^3 Da^{-1} for forms 5 and 6. This higher resolution and also the fact that no native data were available in $P2_12_12$ prompted us to refine the $P2_12_12$ protein model using the *C*2 structure factors. Molecular replacement using the program *CNS* (Brünger *et al.*, 1998) gave two clear solutions for the two monomers. Initial refinement using *CNS*, with no water or NAD, resulted in an *R* factor of 0.25 (R_{free} = 0.33); the refined structure with bound NAD, along with a comparison of crystal packing in forms 5, 6 and 8, will be reported separately.

A. fulgidus cells were kindly provided by H. Monbouquette and I. Schroeder of UCLA. The authors gratefully acknowledge the assistance of Salita Kaistha and Jaya Moses in crystal screening, cultivation and photography. Data for this study were measured at beamline X26c of the National Synchrotron Light Source; financial support for this beamline comes principally from the National Center for Research Resources of the National Institutes of Health and from the Offices of Biological and Environmental Research and of Basic Energy Sciences of the US Department of Energy. Gene-sequence data was provided by the Institute for Genomic Research. Identification of specific instruments and products in this paper is solely to identify the experimental procedure and does not imply recommendation or endorsement.

References

Baker, P. J., Sawa, Y., Shibata, H., Sedelnikova, S. E. & Rice, D. W. (1998). *Nature Struct. Biol.* **5**, 561–567.

Brünger, A. T., Adams, P. D., Clore, G. M., DeLano, W. L., Gros, P., Grosse-Kunstleve, R. W., Jiang, J.-S., Kuszweski, J., Nilges, N., Pannu, N. S., Read, R. J., Rice, L. M., Simonson, T. & Warren, G. L. (1998). *Acta Cryst.* D**54**, 905–921.

Chang, G. G. & Lee, H. J. (1994). *Zool. Stud.* **33**, 177–185.

Galkin, A., Kulakova, L., Ashida, H., Sawa, Y. & Esaki, N. (1999). *Appl. Environ. Microbiol.* **65**, 4014–4020.

Hutter, B. & Singh, M. (1999). *Biochem. J.* **343**, 669–672.

Khaw, L. E., Bohm, G. A., Metcalfe, S., Staunton, J. & Leadlay, P. F. (1998). *J. Bacteriol.* **180**, 809–814.

Klenk, H. P. *et al.* (1997). *Nature (London)*, **390**, 364–370.

McRee, D. (1999). *J. Struct. Biol.* **125**, 156–165.

Pähler, A., Smith, J. L. & Hendrickson, W. A. (1990). *Acta Cryst.* A**46**, 537–540.

Patterson, A. L. (1934). *Phys. Rev.* **46**, 372.

Rao, S. T. & Rossmann, M. G. (1973). *J. Mol. Biol.* **76**, 241–256.

Reddy, P., Peterkofsky A. & McKenney, K. (1989). *Nucleic Acids Res.* **17**, 10473–10488.

Rossmann, M. G. (1972). *The Molecular Replacement Method.* New York: Gordon & Breach.

Schroeder, I., Vadas, A., Johnson, E., Lim, S. & Monbouquette, H. G. (2003). Submitted.

Segovia, L., Horwitz, L., Gasser, R. & Wistow, G. J. (1997). *Mol. Vision*, **3**, 9.

Terwilliger, T. C. & Berendzen, J. (1999). *Acta Cryst.* D**55**, 849–861.